



Thermal expansion and temperature-dependent Young's modulus of Invar fabricated via laser powder-bed fusion

Leonhard Hitzler¹ · Muhammed Zubair Shahul Hameed¹ · Adrian Kah² · Markus Merkel² · Ewald Werner¹

Received: 31 October 2021 / Accepted: 1 April 2022 / Published online: 28 April 2022
© The Author(s) 2022

Abstract

Invar alloys possess the peculiarity of dimensional invariance, which is of importance for high precision applications, such as measurement instruments. As ductile face-centered cubic (fcc) material, it is adequately weldable and is nowadays readily available as powder feed stock for additive manufacturing processes. Single-phase fcc alloys are known to often be highly textured, when fabricated via laser powder-bed fusion. Within this study, the thermal expansion behavior was analyzed via true differential dilatometry and the directional Young's moduli were determined via impulse excitation technique in the temperature range up to 850 °C. The coefficient of thermal expansion was found to be nearly independent of the analyzed orientations. However, Young's moduli differed by 20 GPa, with the highest stiffness obtained for specimens orientated parallel to the x -axis of the machines' coordinate system.

Keywords Additive manufacturing · Selective laser melting · Dilatometry · Inflection temperature · Elastic stiffness · Invar 36

1 Introduction

Powder bed fusion has become one of the most relevant additive manufacturing categories for metal processing. A subcategory, called laser powder-bed fusion (L-PBF), solely utilizes laser beams as primary energy source for local consolidation of the loose powder and includes important processes, such as selective laser melting, direct metal laser sintering and selective laser sintering [1, 2]. These processes essentially differ in the active binding mechanism and hereafter, only full melting of the feedstock in a single step process is considered.

Invar, an alloy consisting of iron and nickel, is well known for its very low thermal expansion [3]. This unique property led to its name, which stems from 'invariant'. The very small thermal expansion of Invar is the result of interaction of a negative magnetostriction opposing thermal expansion [4]. However, this effect is limited to a certain temperature

range. Above 100 °C, the magnetovolume force gradually weakens and at the Curie point (279 °C) the ferromagnetic Invar becomes paramagnetic and exhibits a regular thermal expansion behavior above this temperature [5]. Moreover, the compensation of length change depends on the alloy composition, being most effective for an alloy with 36 wt.-% Ni.

Successful fabrication of Invar via L-PBF was reported in numerous studies, most notably Qiu et al. [6] published an extensive study on the influence of irradiation parameters on relative density, surface morphology and tensile properties. Almost defect-free samples were produced and Invar was found to exhibit good processability for a wide range of scan speeds. In the presence of pores mechanical properties deteriorate, especially true for ductility along the built direction (z -axis). The very high impact on deformability in built direction due to voids is symptomatic for layer-wise processing technologies [1, 7]. With appropriate fabrication parameters, however, laser powder-bed-fused Invar can exhibit a superior ductility in built direction, which indeed is uncommon, but has been reported previously for ductile dental cobalt-based alloys [6, 8]. The explanation for the change in behavior in the absence of stress concentrations at imperfections resides in the microstructure, specifically in the orientation of the crystallographic directions relative to the external load [9, 10]. Crystallographic orientation also

✉ Leonhard Hitzler
leonhard.hitzler@tum.de

¹ School of Engineering and Design, Institute of Materials Science and Mechanics of Materials, Technical University Munich, 85748 Garching, Germany

² Institute for Virtual Product Development, Aalen University of Applied Sciences, 73430 Aalen, Germany

Table 1 Parameter set utilized for fabrication of Invar 36 on a SLM 280HL machine

Scan speed [mm/s]	Laser power [W]	Hatch distance [mm]	Scan vector length [mm]	Rotation angle increment [°]	Limitation window [°]	Layer thickness [μm]
780	200	0.12	5	67	114	30
Miscellaneous settings:		Stripe pattern with bidirectional scanning, nitrogen atmosphere, preheating temperature of 200 °C (substrate plate heating)				

Table 2 Sample orientations, stated as reorientation to the built direction (z-axis)

Orientation	Reorientation relative to z-axis [°]			Comment
	A	B	C	
Horizontal x	0	90	0	Parallel to x-axis
Horizontal y	90	0	0	Parallel to y-axis
45°	45	0	0	45° to substrate plate
Vertical	0	0	0	Parallel to z-axis

impacts Young's modulus and crystal anisotropy, with the Zener anisotropy for Invar reported to be about 3.5 [11, 12].

Within this study, the thermal expansion and temperature dependency in Young's modulus of Invar processed by L-PBF were investigated. Thermal expansion was determined up to 600 °C and the Young's modulus up to 850 °C. To account for the anisotropic material behavior samples in various orientations were considered, i.e. horizontally and vertically aligned samples, as well as samples built with 45° inclination to the substrate plate.

2 Samples and experimental methods

2.1 Sample fabrication

Samples were fabricated from gas atomised Invar 36 powder (1.3912, supplied by SLM Solutions AG) on an SLM 280HL machine (SLM Solutions AG, Lübeck, Germany), equipped with a 400 W Yb-fibre-laser. The fabrication parameters are listed in Table 1. Sample orientations are stated by their longitudinal axis orientation relative to the built direction (z-axis) through the rotation angles (*A*, *B*, *C*), according to the ISO/ASTM 52,921:2019 [13] standard. Samples were fabricated in four distinct orientations, two horizontal directions, one vertical direction and one 45° inclination to the substrate plate (Table 2). Three sample geometries were fabricated, all samples were built with an oversize and were then machined to their final geometry (Table 3). Samples of type I in the 45° inclination are exemplified in Fig. 1.

2.2 Dilatometry

A true differential dilatometer (Bähr DIL 802, TA Instruments, USA) equipped with a resistance furnace (up to 1350 °C) was utilized for thermal expansion characterization. The reference specimen used was a hollow quartz sample with an outer diameter of 4 mm, an inner diameter of 1.5 mm and 50 mm in length. It had a thermal expansion coefficient of 0.5×10^{-6} /K in the temperature range of –193 °C to 727 °C. The samples' temperature was measured with a type K thermocouple positioned on their surface (Fig. 2). The samples (type I) were heated up to 360 °C at a rate of 5 K/min, held at 360 °C for 30 min, followed by furnace cooling. Subsequently, the samples were heated up to 600 °C (rate of 5 K/min), held at this temperature for 30 min, and then were furnace cooled (Fig. 3a). The holding time of 30 min was applied to ensure a stable condition, i.e. constant temperature after an initial temperature overshoot and no detectable fluctuations in the elongation signal. All annealings were performed under vacuum (~50 Pa). Figure 3b depicts a schematic thermal expansion curve between ambient temperature and 600 °C. The inflection temperature ($T_{\text{Inflection}}$) was estimated from the point of intersection of the regression lines¹. The average thermal expansion coefficient above the Curie temperature was obtained via the two holding points, namely at 360 °C and 600 °C, and the corresponding thermal expansion ΔL .

2.3 Impulse excitation technique

The impulse excitation technique (IET) is a reliable method for the precise measurement of elastic moduli. A freely supported sample is excited to vibration by an impulse, allowing to determine its eigenfrequencies from its emitted sound. Eigenfrequencies depend on the sample geometry, the density and the elastic properties of the material. The determination of the elastic moduli is standardized by the ASTM E1876-15 [14] exclusively in case of isotropic elasticity. However, IET can also be applied in case of anisotropic elasticity for the determination of direction-dependent

¹ Regression curves were calculated with the least square method, not to be confused with tangents.

Table 3 Sample types, sample dimensions in machined condition and conducted experiment for each sample type

Sample type	Diameter [mm]	Length [mm]	Number of samples per configuration	Conducted experiment	
I	7	50	5	Thermal expansion, Young’s modulus	
II	10	70	1	Young’s modulus (ambient temperature)	
Sample type	Width [mm]	Thickness [mm]	Length [mm]	Number of samples per inclination	Conducted experiment
III	14	2	65	1	Young’s modulus (elevated temperature)

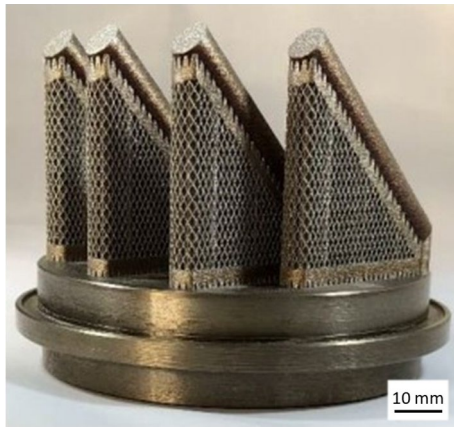


Fig. 1 Fabricated cylindrical samples (type I) with 45° inclination to the substrate plate

elastic moduli, given the sample geometry is suitable, which is particularly relevant for strongly textured materials [15].

In this contribution bar-shaped samples with a high length to thickness ratio were analyzed (Table 3). This allows to estimate Young’s modulus E_1 in the longitudinal direction of the sample from the fundamental flexural eigenfrequency by replacing the isotropic Young’s modulus in the relations from the ASTM E1876-15 [14] standard by E_1 . For cylindrical samples (type I and II), the Young’s modulus is calculated by:

$$E_1 = \frac{1.6067l^3mf_f^2T_1}{d^4}, \tag{1}$$

where f_f denotes the fundamental flexural eigenfrequency, m is the mass of the sample, d denotes the diameter and l the length of the sample. In case of a rectangular cross-section (type III) the following equation is applied:

$$E_1 = \frac{0.9465T_1mf_f^2l^3}{bt^3}, \tag{2}$$

where t denotes the thickness and b the width of the sample. Equations (1) and (2) are based on Euler–Bernoulli’s beam

theory. The correction factor T_1 accounts for the influence of transverse shear deformation in the fundamental flexural eigenmode and is close to one for slender bars.

The RFDA HT1050 setup (IMCA, Genk, Belgium) equipped with a resistance furnace (maximum temperature 1050 °C) was utilized for IET measurements (Fig. 4). All three sample types (Table 3) were measured at ambient temperature, samples of type I were measured before and after the annealing treatment in the dilatometer and samples of type III were measured at elevated temperatures up to 850 °C (heated up from ambient temperature to 850 °C at a rate of 4 K/min, followed by furnace cooling). IET is particularly advantageous for measurements at elevated temperatures, as the entire experiment can be performed in a furnace. Samples with a rectangular cross-section are preferred for measurements at elevated temperatures, as these are shifted less on the supports by the impulse as compared to cylindrical samples.

The accuracy of the result strongly depends on the accuracy of the sample dimensions, which have been measured with a micrometer screw at several positions for each sample. Averaged values were used for the calculation of E_1 , whereby the observed dimensional variations allowed to estimate the impact of dimensional deviations by linear error propagation (Table 4). The dimensional variations of the samples were similar, about 0.01 mm deviation in thickness, width, diameter and length. A further impact on the accuracy of the calculated Young’s modulus stemmed from the formation of an oxide layer at elevated temperatures, which led to moderate changes of the sample geometry.

3 Results and discussion

3.1 Thermal expansion behavior

Samples consistently showed a small negative expansion in the temperature range of up to 100 °C to 150 °C, followed by a slow onset of positive elongation. An initially negative thermal expansion has been documented for laser

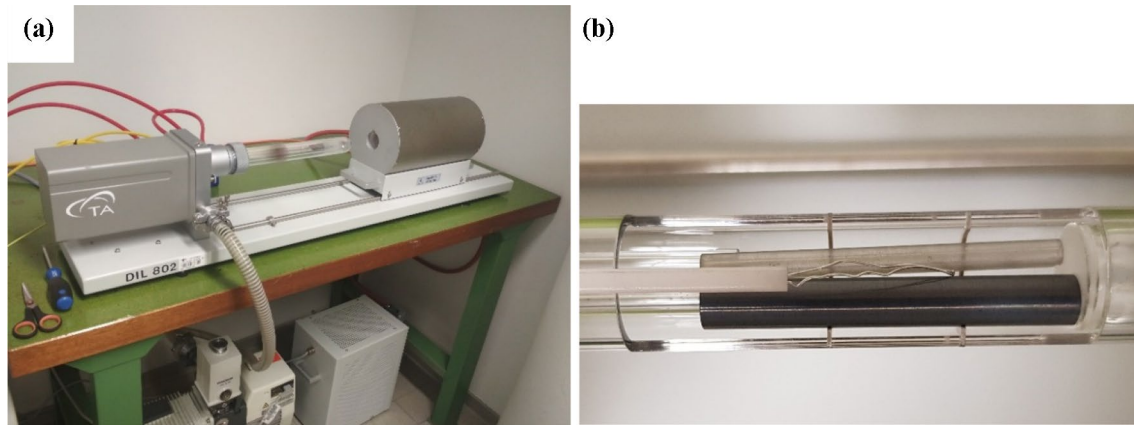


Fig. 2 **a** Dilatometer DIL 802 equipped with resistance furnace and **b** detailed sample placement with quartz reference sample and type K thermocouple

powder-bed-fused Invar before by Harrison et al. [5], however, it is an atypical behaviour for Invar. No negative expansion has been reported by Asgari et al. [16], who also investigated Invar samples fabricated via L-PBF.

The inflection temperature ($T_{\text{Inflection}}$) was estimated to range from 257 °C to 264 °C (Table 5). Considering the standard deviation of the data, $T_{\text{Inflection}}$ was similar for all investigated orientations and hence, no noteworthy directional dependency was evident. The inflection temperature in this study was about 35 °C higher compared than that stated in the study by Yakout et al. [17] (225 °C), who utilized an induction coil for heating in an atmosphere of helium atmosphere, but investigated considerably shorter samples with just 10 mm in length. However, the thermal expansion coefficient reported by Yakout et al. [17] and this Invar study are nearly the same. Furthermore, the coefficient of thermal expansion, α , seemed to be the same irrespective of the specimen orientation.

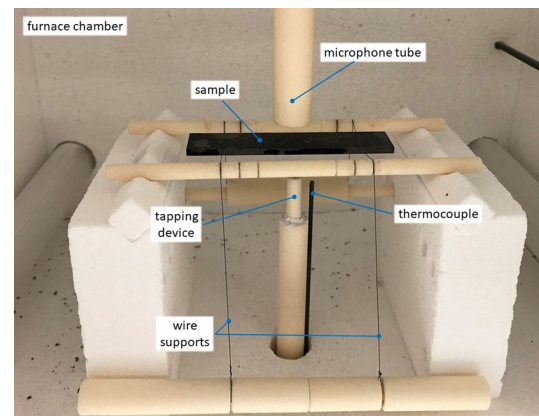


Fig. 4 IET setup inside furnace, showing a sample of type III placed on the wire supports

In contrast to other investigations, which often report the thermal expansion behaviour during cool-down, this

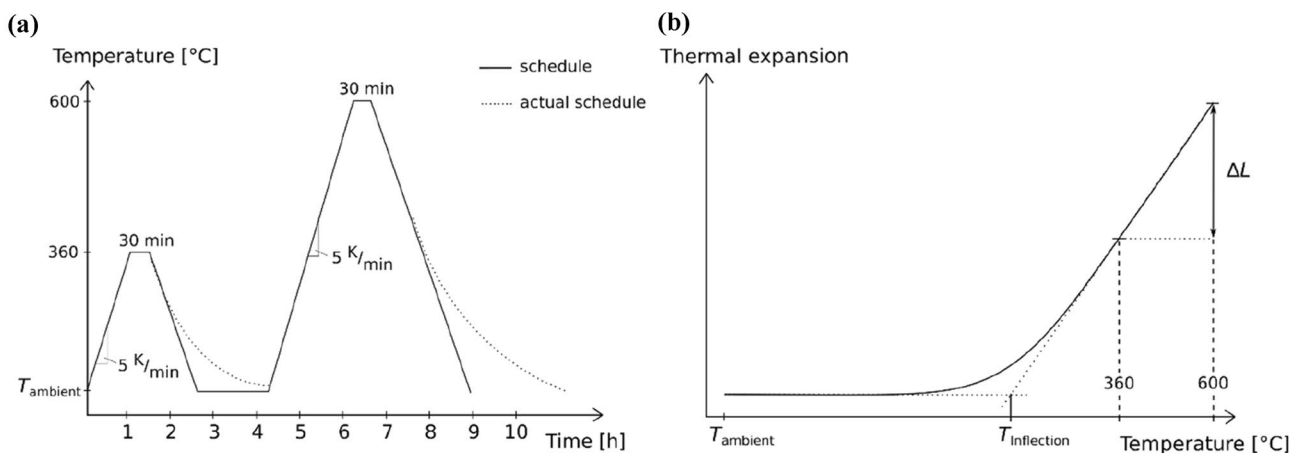


Fig. 3 **a** Annealing cycle during dilatometer testing; **b** evaluation schematic

Table 4 Expected deviations for E_1 due to dimensional deviations, based on the linear error propagation at $E_1 = 150\text{GPa}$

	Type I	Type II	Type III
$ \Delta E_1 $ in [GPa]	0.95	0.66	2.42

study considers the first heat-up phase [11]. The approach to consider the heat-up phase has the apparent detriment of waviness in the data, caused by the pulsed regulation of the furnace. However, for equipment fabricated via L-PBF and put in operation, the heat-up run is believed to be more relevant in practice.

3.2 Young's modulus

Young's moduli for sample types I and II were the same when testing the same orientation. The respective values for sample type III were slightly lower than the aforementioned ones. The highest Young's modulus of approximately 150 GPa was observed for horizontal samples aligned parallel to the x -axis². For all other investigated orientations, Young's modulus was about 130 GPa with low scatter of the individual results (Table 6). It should be noted that the disparity of horizontally aligned samples—150 GPa in x -direction and 130 GPa in y -direction—is omitted in the material data sheet [18].

Deviations of Young's moduli before and after annealing treatments were low. Samples of type I exhibited on average a difference of about 0.5 GPa between the Young's moduli in their as-built state compared to the one after annealing at 600 °C, with similar scatter in the obtained results. Taking the uncertainty into account, resulting from dimensional deviations, the results for samples of type I remained unaffected by annealing.

Samples of type III were more sensitive to annealing. On average, Young's modulus increased by approximately 5 GPa after annealing at 850 °C. The consistent gain in Young's modulus for samples of type III is assumed to largely stem from the oxide layer formed during annealing. Rectangular shaped samples also are more prone to discrepancies caused by changes in thickness than their cylindrical counterparts, due to the disproportionate mass distribution over their cross-section. This sensitivity was also evident in the estimated deviations for the individual sample types (Table 4), which was largest for samples of type III, although the dimensional deviations of all sample types were similar (~0.01 mm). In conclusion, very low changes in Young's modulus due to annealing have been found, which is in line

with the results of Qiu et al. [6], according to which no significant changes in microstructure and tensile strength are to be expected after annealing Invar 36 samples at temperatures up to 830 °C.

Up to a temperature of approximately 240 °C, Young's modulus steadily increased, after which it showed a maximum between 260 °C and 270 °C, which was followed by a monotonic decrease thereafter (Fig. 5). The respective maxima and minima (at 850 °C) of Young's modulus determined for differently aligned samples of type III are listed in Table 7. The monotonic decrease in Young's modulus above 260 °C to 270 °C with increasing temperatures is to be expected, since an increased interatomic distance reduces the stiffness of the crystal lattice [19].

Comparing the curves of both thermal expansion and Young's modulus as function of temperature (Fig. 6), the tendencies aligned. In the temperature range, ambient temperature to approximately 150 °C, the magnetovolume force counteracted thermal expansion. Since, however, the endeavor for thermal expansion is still present and, in turn resembles a force, the materials' stiffness needs to increase to form an equilibrium without a macroscopic measurable expansion. In this regard, the increasing magnetovolume force appears to gradually increase the Young's modulus. Considering that the thermal expansion was found to be independent from the sample orientation, it appeared viable that the stiffening was also found independent from the orientation. Young's modulus increased by approximately 20 GPa in the temperature range from 25 °C to its respective maximum, irrespective of the sample orientation.

While the thermal expansion gradually increased, the Young's moduli stagnated, whereby as a result $T_{\text{Inflection}}$ and the temperatures at which the maxima in Young's modulus occurred, coincided. Above 300 °C, Invar 36 exhibited the common behavior of most metals, with an approximately linear increase in thermal expansion, while Young's modulus steadily decreased.

On close inspection, all three Young's modulus progression curves showed a slightly higher gradient in the increase in Young's modulus between 220 °C and 230 °C. However, no coinciding effect was evident in the thermal expansion data and no final conclusion could be drawn.

4 Conclusion

Thermal expansion and Young's moduli of laser powder-bed-fused Invar 36 were analyzed via dilatometry and impulse excitation (IET) method in the temperature range up to 850 °C. While Invar 36 fabricated with L-PBF is known to show macroscopic anisotropy in its mechanical properties,

² The x -axis corresponds to the recoater transition axis in the employed SLM 280HL machine.

Table 5 Results of thermal expansion analysis on type I samples, stated as average value. STDEV denotes the standard deviation

Orientation	Approximate begin of thermal expansion [°C]*		Inflection temperature $T_{\text{Inflection}}$ [°C]		Thermal expansion coefficient α [$10^{-6}/\text{K}$]**	
	Average	STDEV	Average	STDEV	Average	STDEV
Horizontal x	190	7.9	261	7.9	16.4	0.21
Horizontal y	178	11.5	257	9.2	16.5	0.18
45°	186	8.2	264	7.1	16.7	0.07
Vertical	185	8.7	257	4.7	16.4	0.39

*Temperature of onset of noticeable thermal expansion

**In the temperature range 360 °C to 600 °C

Table 6 Young’s moduli at ambient temperature (~25 °C) before and after heat treatment

Sample type	Orientation	Young’s modulus E [GPa]		Young’s modulus E [GPa] after annealing treatment*	
		Average	STDEV	Average	STDEV
I	Horizontal x	150.18	0.53	149.54	0.48
II		150.35	–	–	–
III		148.65	–	154.17**	–
I	Horizontal y	130.66	0.58	131.24	0.61
II		129.51	–	–	–
III		126.28	–	131.72**	–
I	45°	131.21	1.62	131.25	1.63
II		133.21	–	–	–
III		130.92	–	135.15**	–

*600 °C for type I and 850 °C for type III

**Oxide layer formed on samples’ surface

Table 7 Selected values for Young’s modulus determined by IET in the temperature range from 25 °C to 850 °C for samples of type III. 25 °C: ambient temperature; 260 °C to 270 °C: temperature of maximum in Young’s modulus; 850 °C: maximum temperature reached in the experiments

Orientation	Young’s modulus E [GPa]	Temperature [°C]
Horizontal x	148.65	25
	167.71	260
	137.60	850
Horizontal y	126.28	25
	145.09	270
	119.32	850
Vertical	130.92	25
	148.80	265
	122.28	850

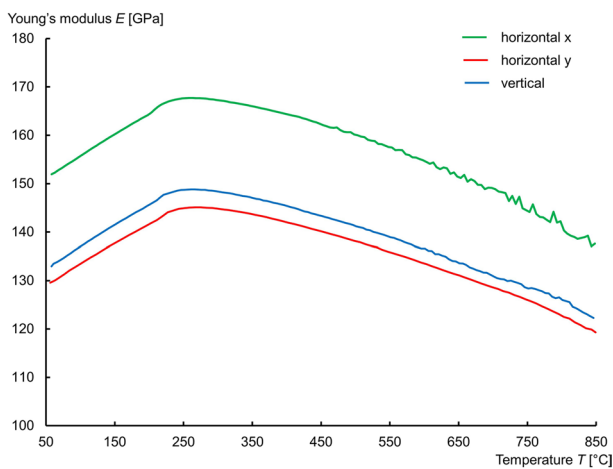


Fig. 5 Temperature dependency of Young’s modulus, determined from IET results for sample type III

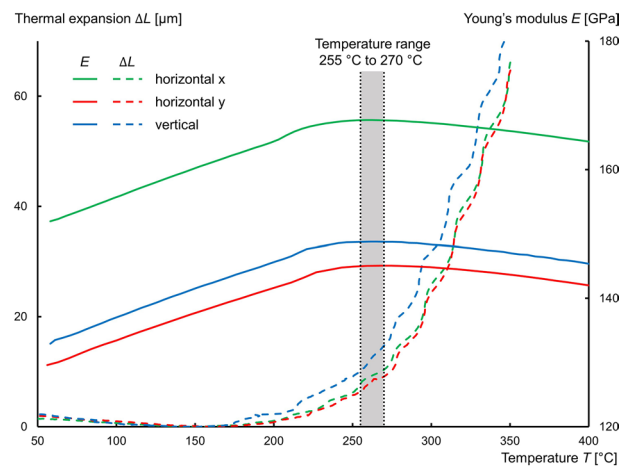


Fig. 6 Comparison of thermal expansion (samples of type I) and Young’s modulus (samples of type III); $T_{\text{Inflection}}$ and the maxima of E are located between 255 °C and 270 °C for all specimen orientations

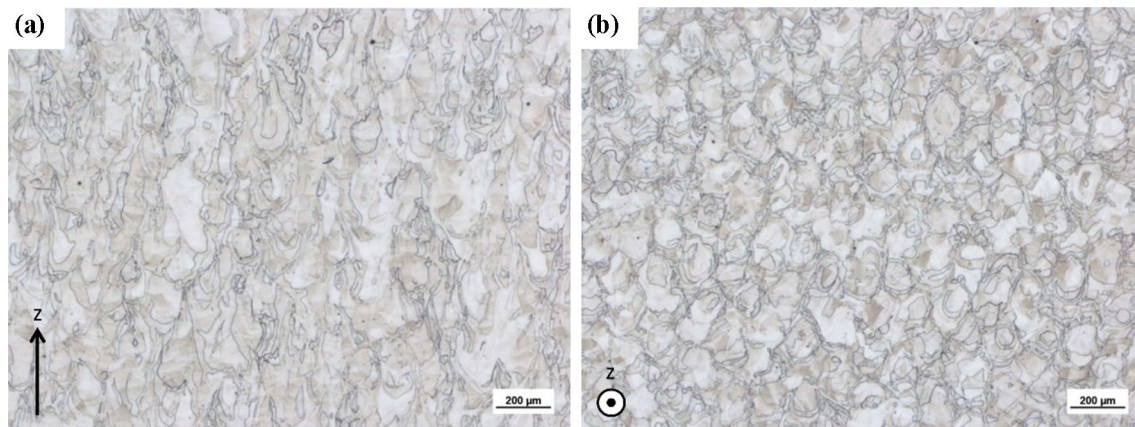


Fig. 7 Etched micro sections of a horizontal x sample of type I **a** cross-sectional cut and **b** longitudinal cut parallel to the layering

which was confirmed by its direction-dependent Young's modulus, the temperature dependencies of both thermal expansion and Young's modulus appear to be independent from the orientation. The Young's modulus ranged from 130 GPa to 150 GPa, with the maximum being present along the horizontal x -direction. However, comparing the recorded maxima of Young's modulus just below the Curie temperature (279 °C) with the respective value at ambient temperature, the gain in Young's modulus was approximately 20 GPa for all orientations tested. Thus, the increase in Young's modulus was found to be independent from the orientation, which similarly was the case for the thermal expansion behavior. In this instance, the coefficient of thermal expansion and the temperature of inflection can be treated as direction independent statistical values, with a thermal expansion above 300 °C of $16.5 \times 10^{-6}/\text{K}$, and a temperature of inflection of 260 °C.

For lower temperatures of up to 150 °C, a slight negative thermal elongation has been recorded, which at this point cannot be explained and available data from already published data on this fluctuates. Further studies will be required to clarify the origin of this atypical behavior.

Appendix

The section "Appendix" contains further details to supplement the given information and evaluation in the main section and to allow for repetition and thorough comparisons.

Metallographic investigations were conducted on a horizontal x sample of type I. The microstructure showed elongated grains in the cross-sectional cut (Fig. 7). The elongation corresponds with the built direction and the grains grew through multiple layers. The microstructure was almost defect-free, with only a few pores $< 10 \mu\text{m}$ being present.

Acknowledgements Sincere appreciation to Thomas Obermayer for his kind support and effort in sample preparation and the implementation of the impulse excitation technique, including evaluation of the data. The authors further thank Josef Tomas and Michael Sedlmajer for their kind support in the sample fabrication and the coordination within the laboratories.

Funding Open Access funding enabled and organized by Projekt DEAL.

Declarations

Conflict of interest The authors declare that there is no conflict of interest.

Open Access This article is licensed under a Creative Commons Attribution 4.0 International License, which permits use, sharing, adaptation, distribution and reproduction in any medium or format, as long as you give appropriate credit to the original author(s) and the source, provide a link to the Creative Commons licence, and indicate if changes were made. The images or other third party material in this article are included in the article's Creative Commons licence, unless indicated otherwise in a credit line to the material. If material is not included in the article's Creative Commons licence and your intended use is not permitted by statutory regulation or exceeds the permitted use, you will need to obtain permission directly from the copyright holder. To view a copy of this licence, visit <http://creativecommons.org/licenses/by/4.0/>.

References

1. Hitzler L, Merkel M, Hall W, Öchsner A (2018) A review of metal fabricated with laser- and powder-bed based additive manufacturing techniques: process, nomenclature, materials, achievable properties, and its utilization in the medical sector. *Adv Eng Mater* 20:1700658
2. ISO/ASME International (2015) ISO/ASTM 52900. Additive manufacturing-general principles-terminology. ISO/ASME International, Geneva
3. Corbacho JL, Suárez JC, Molleda F (1998) Welding of invar Fe-36Ni alloy for tooling of composite materials. *Weld Int* 12:966–971

4. Rancourt DG, Dang M (1996) Relation between anomalous magnetovolume behavior and magnetic frustration in Invar alloys. *Phys Rev B Condens Matter* 54:12225–12231
5. Harrison NJ, Todd I, Mumtaz K (2017) Thermal expansion coefficients in Invar processed by selective laser melting. *J Mater Sci* 52:10517–10525
6. Qiu C, Adkins NJE, Attallah MM (2016) Selective laser melting of Invar 36: microstructure and properties. *Acta Mater* 103:382–395
7. Hitzler L, Hirsch J, Heine B, Merkel M, Hall W, Öchsner A (2017) On the anisotropic mechanical properties of selective laser melted stainless steel. *Materials* 10:1136
8. Hitzler L, Alifui-Segbaya F, Williams P, Merkel M, Heine B, Heitzmann M, Hall W, Öchsner A (2018) Additive manufacturing of cobalt-based dental alloys: analysis of microstructure and physicochemical properties. *Adv Mater Sci Eng* 2018:8213023
9. Wang X, Muñoz-Lerma JA, Attarian Shandiz M, Sanchez-Mata O, Brochu M (2019) Crystallographic-orientation-dependent tensile behaviours of stainless steel 316L fabricated by laser powder bed fusion. *Mater Sci Eng A* 766:138395
10. Fischer T, Hitzler L, Werner E (2021) Morphological and crystallographic effects in the laser powder-bed fused stainless steel microstructure. *Curr Comput-Aided Drug Des* 11:672
11. Masumoto H, Kikuchi M, Sawaya S (1970) Elastic anisotropy and its temperature dependence of single crystals of 63% Fe-32% Ni-5% Co alloy (super-invar). *Trans Jpn Inst Met* 11:176–179
12. Zener C (1948) Elasticity and anelasticity of metals. The University of Chicago Press, Chicago
13. Deutsches Institut fuer Normung e.V. (DIN) (2019) DIN EN ISO/ASTM 52921. Additive fertigung—grundlagen—standardpraxis der positionierung, koordinaten und ausrichtung des bauteils. Beuth Verlag, Berlin
14. ASTM International (2001) E1876–15. Standard test method for dynamic young's modulus, shear modulus, and poisson's ratio by impulse excitation of vibration. ASTM International, West Conshohocken. <https://doi.org/10.1520/E1876-15>
15. Obermayer T, Kremaszky C, Werner E (2021) Determination of the anisotropic elasticity tensor by mechanical spectroscopy. *Cont Mech Thermodyn* 34(1):165–184
16. Asgari H, Salarian M, Ma H, Olubamiji A, Vlasea M (2018) On thermal expansion behavior of invar alloy fabricated by modulated laser powder bed fusion. *Mater Des* 160:895–905
17. Yakout M, Elbestawi MA, Veldhuis SC (2018) A study of thermal expansion coefficients and microstructure during selective laser melting of Invar 36 and stainless steel 316L. *Addit Manuf* 24:405–418
18. SLM Solutions Material data sheet: Fe-alloy Invar 36 / 1.3912. SLM solutions. https://www.slm-solutions.com/fileadmin/Content/Powder/MDS/MDS_Fe-Alloy_Invar36_0219_EN.pdf. Accessed 27/10/2021
19. Husain A, La P, Hongzheng Y, Jie S (2020) Influence of temperature on mechanical properties of nanocrystalline 316L stainless steel investigated via molecular dynamics simulations. *Materials* 13:2803

Publisher's Note Springer Nature remains neutral with regard to jurisdictional claims in published maps and institutional affiliations.